Phase Identification in a Series of Liquid Crystalline TPP Polyethers and Copolyethers Having Highly Ordered Mesophase Structures. 1. Phase Diagrams of Odd-Numbered TPP Polyethers

Yeocheol Yoon, Anqiu Zhang, Rong-Ming Ho, and Stephen Z. D. Cheng*

Maurice Morton Institute and Department of Polymer Science, The University of Akron, Akron, Ohio 44325-3909

Virgil Percec and Peihwei Chu

Department of Macromolecular Science, Case Western Reserve University, Cleveland, Ohio 44106-2699

Received February 24, 1995; Revised Manuscript Received September 26, 1995[⊗]

ABSTRACT: A series of liquid crystalline polyethers has been synthesized from 1-(4-hydroxy-4′-biphenylyl)-2-(4-hydroxyphenyl)propane and α,ω-dibromoalkanes [TPP(*n*)]. From the differential scanning calorimetry experiments, the TPP(*n*=odd)s show multiple phase transitions during cooling and heating. For each TPP(*n*=odd) the supercooling dependence of these transitions is found to be small. A phase diagram of the transition temperatures and the enthalpy and entropy changes of the transitions with respect to the number of methylene units (*n*) for TPP(*n*=odd)s have been obtained. Analyses have been conducted regarding the contributions of both the mesogenic groups and the methylene units to the differently ordered structures. Identification of the ordered structures in each phase has been carried out by combining wide angle X-ray powder and fiber diffraction experiments at different temperatures with polarized light and transmission electron microscopy experiments on the liquid crystal morphology and defects. It is found that for TPP($n \leq 13$)s the highest temperature transition is from the isotropic melt to a nematic phase. However, for TPP($n \geq 15$)s, the isotropic melt directly converts to a smectic F phase having a monoclinic unit cell (a pseudohexagonal packing tilted toward a side). The WAXD fiber patterns for this phase show that the chain orientation is parallel to the fiber direction. For TPP($n \leq 13$)s formation of a smectic F phase with a monoclinic unit cell from the nematic phase can also be determined and the WAXD fiber pattern shows that the chain orientation is at an angle ranging between 0 and 20° with respect to the fiber direction. With an increase in the number of methylene units, this angle gradually decreases until $n = 15$, where this angle becomes zero. Further cooling leads to a smectic crystal G phase for all TPP(*n*=odd)s, and the different chain orientations with respect to the fiber direction in the WAXD fiber patterns still exist. TPP($n \leq 9$)s remain in the smectic crystal G phase down to their glass transition temperatures, while TPP($n \geq 11$)s form a smectic crystal H phase (a tilted herringbone, orthorhombic packing tilted toward the *b*-axis side, and $a > b$) in a low temperature range.

Introduction

During the last two decades, mesophase identification and the transition behaviors in main-chain liquid crystalline polymers have been extensively studied.[1] In most of the cases, liquid crystalline polymers are enantiotropic, and a nematic phase is found above the crystal melting temperature. Recently, some publications have reported the existence of a smectic A or C phase (S_A or S_C).[2−7] This is mainly based on the layer structure appearing at the low-angle region of the wide angle X-ray diffraction (WAXD) experiments (powder and fiber patterns). Within the layers, the lateral structure shows a short range order (liquid-like lateral packing having a typical correlation length of less than 2 nm). Most of these smectic phases are directly formed from the isotropic melt, and it is expected that the formation of layer structure may be closely associated with the microscopic separation of the methylene units from the mesogenic groups.

There are many fundamental aspects in the research area of main-chain liquid crystalline polymers. At least two of them are interesting to us. First, what is the molecular aspect and kinetics of the formation of the smectic liquid crystalline phase? This kind of phase formation is usually close to thermodynamic equilibrium. The transition kinetics is very fast and difficult to study experimentally. In order to slow down the transition kinetics, one cannot expect to have a high transition energy barrier as in the case of polymer crystallization but, instead, one has to design liquid crystalline polymers which possess a glass transition close to their liquid crystalline transition temperatures. As a result, a decrease of the molecular motion leads to a suppression of the liquid crystalline transition kinetics.[6] However, at this moment a systematic conclusion regarding this kind of transition kinetics is certainly still a distance away from our full understanding.

The second aspect is that, can we identify smectic phases having an order higher than S_A or S_C in main-chain liquid crystalline polymers? A few years ago, smectic E- and B-like phases were proposed by Yoon *et al.* to describe liquid crystalline aromatic polyester and copolyesters.[8] On the other hand, smectic crystal phases have also been identified in the main-chain liquid crystalline polyesters.[9,10] The highly ordered smectic crystal phases exhibit a certain degree of lateral order (quasi-long range having a typical correlation length of 3−9 nm or, long range order having a typical correlation length of larger than 10 nm in polymers) in addition to the layer structure. These mesophases may be further ordered to form smectic crystals when

* To whom the correspondence should be addressed.
⊗ Abstract published in *Advance ACS Abstracts,* December 1, 1995.

0024-9297/96/2229-0294$12.00/0

positional order is introduced within, or even among, the layers. The difference between small molecule and main-chain liquid crystalline polymers in these smectic phases is the molecular connectivity between the layers in the polymers. This connectivity does not exist in small molecule liquid crystals.

Recently, in order to search for the possibility of the liquid crystalline polymers involving highly ordered smectic phases, a series of liquid crystalline polyethers has been synthesized from 1-(4-hydroxy-4′-biphenylyl)-2-(4-hydroxyphenyl)propane and α,ω-dibromoalkanes. They are abbreviated as TPPs.[11] The chemical structure of these polyethers is

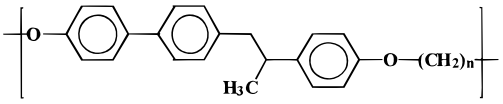

In this publication, we focus on the phase behavior of the odd-numbered TPPs [TPP(n=odd)s]. We employed differential scanning calorimetry (DSC) to investigate the transition thermodynamics, WAXD to follow structural developments and identify new phases during the transitions, and polarized light and transmission electron microscopy (PLM and TEM) to study phase morphological changes and liquid crystalline defects. Interestingly, it is found that in these polyethers the smectic phases observed possess ordered structures higher than S_A or S_C, namely, their lateral packing is higher than the short range liquid-like order. Furthermore, multiple mesophase transitions are observed during cooling from the isotropic melt and the degree of order in these phases progressively increases.

Experimental Section

Materials. TPP(n=odd)s were synthesized from 1-(4-hydroxy-4′-biphenylyl)-2-(4-hydroxyphenyl)propane (TPP) and α,ω-dibromoalkanes. The detailed synthetic procedure has been reported in an earlier publication.[11] In brief, the starting material for the mesogenic group (TPP) was 4-phenylphenol (**1**) and (4-methoxyphenyl)acetic acid (**2**). 4-Acetoxybiphenyl (**3**) was prepared by the esterification of **1**, and (4-acetoxyphenyl)acetic chloride (**4**) was from the demethylation and esterification of **2**. 1-(4-Acetoxy-4′-biphenylyl)-2-(4-acetoxyphenyl)ethanone (**5**) was prepared by the Friedel−Craft acylation of **2** and **4**. TPP was then synthesized by the methylation, reduction, and demethylation of **5**. Finally, the phase-transfer-catalyzed polyetherification was used to synthesize the polyethers of TPP with α,ω-dibromoalkanes. This was completed under a nitrogen atmosphere at 80 °C in a *o*-dichlorobenzene-10 mol/L NaOH two-phase system using TBAH as a phase-transfer catalyst. The molar ratio of nucleophilic to electrophilic monomers was always 1.0:1.0. Molecular weights of TPP(n=odd)s were determined *via* gel permeation chromatography (GPC) based on polystyrene standards, and they ranged between 20 000 and 30 000.

Instrument and Experiments. DSC experiments were carried out in a Perkin-Elmer DSC-7. The temperature and heat flow scales at different cooling and heating rates (2.5−40 °C/min) were carefully calibrated using standard materials. Typically, the DSC sample size was 2−3 mg. When fast cooling and heating rates were applied, the sample weight was reduced to less than 0.5 mg to avoid a thermal gradient within the samples. The samples were heated to above their melting temperatures for 2 min and then cooled to below the glass transition temperature at different rates. The consecutive heating was also performed at a rate which is equal to, or faster than, the prior cooling rate. When the DSC cooling curves were used to analyze the transition behavior, the onset temperature of the transition in the high-temperature side was determined. When the heating curves were used, the onset temperature was found from the low-temperature side. In both cases the analysis also required recognition of the peak temperatures. When the peaks were overlapped, those were resolved using the PeakFit program published by Jandel Scientific. An asymmetric double sigmoidal function was used for the peak resolution.

Wide angle X-ray diffraction (WAXD) experiments were performed on a Rigaku 12 kW rotating anode generator (Cu Kα radiation) equipped with a diffractometer. A hot stage was set up on the diffractometer to study the structural changes during the phase transition at constant cooling and heating rates. The temperature can be controlled to better than ±1 deg. Thin films having a thickness of 0.1 mm were prepared for the WAXD powder experiments. Fibers were also spun from the isotropic melt in order to identify the phase structure. A typical fiber diameter was 30 μm, and the fibers were quenched to room temperature after spinning and annealing at different temperatures, which were usually 5−10 deg below the transition temperature measured from DSC. The TPP thin film samples were scanned in a 2θ angle region between 2 and 35°. The scanning rate was 20°/min. The thermal histories of the samples were kept the same as those in the DSC experiments. The WAXD fiber patterns were also taken at different temperatures, particularly at those temperatures where the phase transitions occur, *via* a Siemens two-dimensional area detector with built in hot stage. About 0.5 h was required to obtain a high-quality WAXD fiber pattern. The fiber length was fixed during the experiments. According to the Scherrer equation, the width at half-peak height of each reflection peak is reciprocally proportional to the correlation length of the ordered structure perpendicular to the reflection plane.

Liquid crystalline morphology was examined *via* a PLM (Olympus BH-2) with a Mettler hot stage (FP-82). Both isothermal and nonisothermal experiments were performed. When the cooling and heating rates were used, they were always kept the same as those applied in DSC and WAXD experiments. The samples were vacuum-dried solution-cast films prepared from a 2% solution of polymer in chloroform. In order to study the liquid crystalline morphological changes under an external force field, TPP samples were placed between two glass slides and were mechanically sheared.

Liquid crystalline morphology and defect observations were also carried out through a JEOL JEM-120U TEM at an accelerating voltage of 120 kV. The samples were prepared in the same way as in the PLM experiments and then were physically over-sheared to separate the glass slides and immediately quenched. The samples were reheated to a temperature 10−20 deg below the mesophase transition temperature for further annealing. The annealing temperature was carefully selected since one needs to retain the chain orientation induced during shearing and, therefore, lamellar morphology could grow to indicate the chain orientation. This method has been known as the "lamellar decoration method", and it was first proposed by Thomas *et al.*[12,13] to identify liquid crystal polymer defects. The samples were then coated by heavy metals (Au/Pt 0.4/0.6, 30° tilted to the sample surface) and carbon (90° to the sample surface). Finally, the TPP samples were dissolved in a trifluoroacetic acid and chloroform mixture, and the replicas were picked up on TEM grids in distilled water. In order to determine the chain molecular direction, the sheared and coated samples were also directly examined by electron diffraction experiments under the TEM.

Results and Discussion

Thermodynamic Behavior of the Phase Transitions. Figure 1a shows a series of DSC cooling and heating curves for TPP(n=7) at different rates as examples. Multiple phase transitions are exhibited in all cases. The results illustrate little supercooling dependence in these phase transitions which may imply that these transitions are close to thermodynamic equilibrium. Two transition peaks are clearly observed

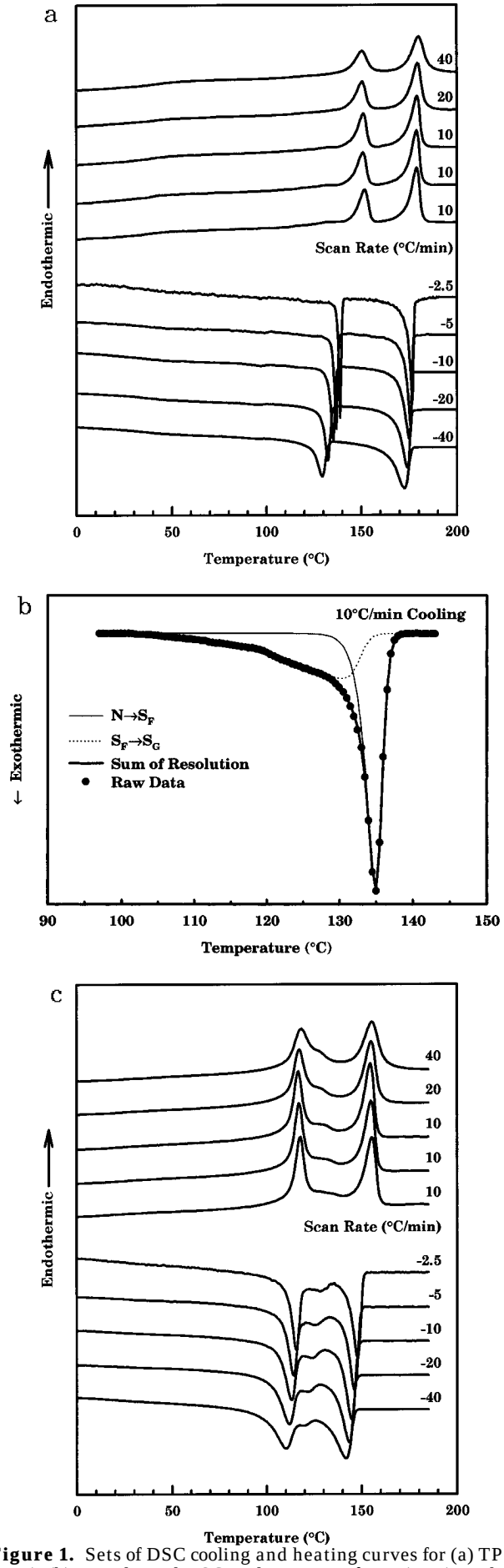

Figure 1. Sets of DSC cooling and heating curves for (a) TPP-(n=7), (b) an enlarged DSC cooling trace of TPP(n=7), and (c) TPP(n=15).

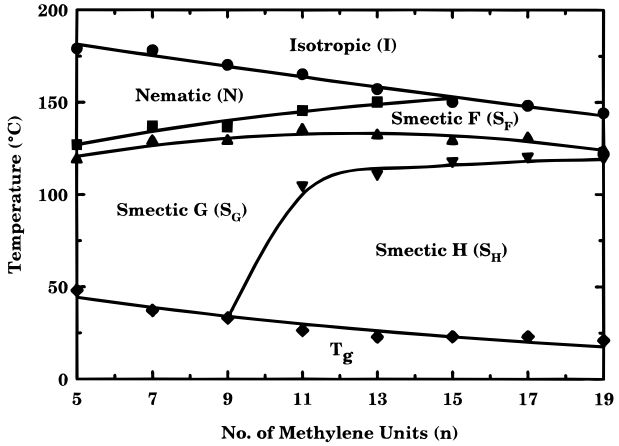

Figure 2. Phase diagram of TPP(n=odd)s.

and followed by a very weak peak around 129 °C (see the magnified DSC curve in Figure 1b). In order to ensure the existence of this transition, over 10 independent DSC runs have been carried out and the transition peak is very reproducible. For the highest transition temperature around 178 °C, the change of cooling rate from 2.5 to 40 °C/min only leads to a 1.4 supercooling. The second transition peak at around 137 °C shows a 7 deg supercooling difference while the lowest phase transition also possesses the same supercooling dependence. Similar observations can also be found in other TPP(n=odd)s. For example, in the case of TPP(n=11), three clear exothermic transitions can be found at 165, 146, and 105 °C. Their supercoolings in the cooling rate range between 2.5 and 40 °C/min are 2, 5, and 2 deg, respectively. There is another minor transition at 135 °C with a 7 deg supercooling dependence, which also represents the structure change (see below). For TPP(n=15), three transitions at 150, 129, and 118 °C possess supercoolings in the same cooling rate range which are 4, 8, and 6 deg, respectively. Extrapolating to zero cooling or heating rate for every TPP(n=odd) provides equilibrium transition temperatures which are used to construct the phase diagram as shown in Figure 2 (the detailed phase structure assignments will be given later). In order to have an overview of the transition behaviors in TPP(n=odd)s, Figure 3 shows a set of DSC cooling curves for TPP(n=odd)s at 5 °C/min. As shown in this figure, the thermal transition behaviors of the TPP($n \leq 9$)s are similar, as are those of TPP($n \geq 15$)s. TPP(n=11 and 13)s seem to be intermediate cases.

Structure Developments during the Phase Transitions. To observe the structure and order change at each phase transition temperature, WAXD experiments were carried out at cooling and heating rates of 5 °C/min. Parts a−c of Figure 4 show three sets of WAXD powder patterns for TPP(n=7, 11, and 15)s at different temperatures during cooling. Since these transitions have little supercooling dependence, the WAXD heating patterns are almost identical to those recorded during cooling. At the highest transition temperature of 178 °C for TPP(n=7), the change of the diffraction patterns from the isotropic melt (I) is only the shift of the d-spacing of the halo at $2\theta = 18.5(0)°$ toward a smaller spacing (the 2θ angle shifts to a higher angle). No other reflection peaks appear during this transition. The d-spacing of the halo represents an average distance among chain backbones. The shift observed in the WAXD powder patterns is an indication of a nematic liquid crystalline (N) transition from the isotropic melt,

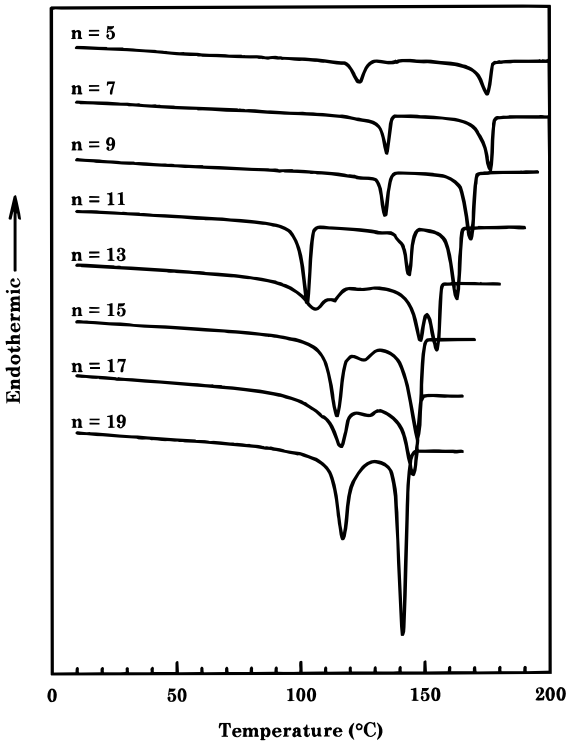

Figure 3. Set of DSC cooling curves for TPP(n=odd)s at a cooling rate of 5 °C/min.

which has been experimentally documented in several liquid crystalline polymers.[14,15] This d-spacing shift can also be observed in other TPP($n \leq 13$)s, indicating that these polyethers possess an I → N transition, which corresponds to the highest temperature transition in DSC results (Figure 1a,b and 3). The results of d-spacing changes with temperature for TPP($n \leq 13$)s are shown in Figure 5. This conclusion is supported by the PLM observations (see below). The d-spacing shift is also observed at the highest transition temperatures observed from DSC for TPP($n \geq 15$). However, it is accompanied by the appearance of other strong reflection peaks at the low and high 2θ angles. For example, in TPP(n=15) an additional reflection at the low-angle region as well as three reflection peaks in the wide angle region appear (Figure 4c). In most of the cases, this kind of low-angle reflection represents a layer spacing in the mesophase structure, and the reflections appearing in the high-angle region should be attributed to the structural order within, and even among, the layer structures. As a result, a smectic phase having a highly ordered structure may possibly form during this transition (see below).

On further cooling TPP(n=7) passes through the second exothermic peak at 137 °C (observed *via* DSC) and goes into a new phase having a narrow temperature range of about 10 deg. This leads to an appearance of a reflection peak at around $2\theta = 19-20°$. In fact, this peak seems to be a merge of two sharp reflection peaks having very close 2θ values (see below). This kind of transition behavior can be found in TPP(n=odd)s, up to $n = 13$, just below the nematic transition during cooling (see Figure 2). At this transition low-angle reflections in WAXD powder patterns are recognizable but are not well developed for TPP($n \leq 9$)s. On the other hand, the low-angle reflections are well developed for TPP(n=11 and 13). This phase for TPP($n \leq 13$)s actually joins the phases of TPP($n \geq 15$)s formed after the highest transition temperatures. Although their WAXD powder patterns are apparently different, it will be shown that this difference is caused by the orientation of the chain direction rather than the structural order (see below).

The lowest transition observed in TPP($n \leq 9$)s only possesses a weak enthalpy change observed from DSC. The ordered structure after this transition is represented by two overlapped sharp reflection peaks in the WAXD powder patterns appearing at close reflection angles between $2\theta = 19$ and 20°. Other weak reflections are also seen (see Figure 4a). Surprisingly enough, TPP(n=11 and 13) also show similar thermal behaviors and structural development during their third transitions to join those of TPP($n \leq 9$)s. The only apparent difference is that the major reflection peak in the 2θ range of 19−20° becomes narrower with the increasing number of methylene units (Figure 4b). On the other hand, after the second transition temperature is passed during cooling for TPP($n \geq 15$)s (Figure 2), the WAXD powder patterns in a temperature range of about 10−20 deg also show a further ordering process which is represented by increasing the reflection intensities and the appearance of additional reflections. Furthermore, the 2θ angles of their reflections are also changed. Apparently, the WAXD powder patterns in this temperature region are slightly different from those of TPP($n \leq 13$)s since only one major, sharp reflection peak (Figure 4c) can be observed within the 2θ range of 19−20° instead of two overlapping two reflection peaks. However, detailed X-ray analysis will show that they also belong to the same phase as those found in TPP($n \leq 13$)s (see below). The low-angle reflection in this case is always sharp and strong.

For TPP($n \geq 11$)s major enthalpy changes at the lowest transition temperatures are observed *via* DSC, the multiple reflections on the WAXD powder patterns in the high-angle region possess similar patterns. Therefore, the ordered structures developed during this transition for TPP($n \geq 11$)s should be close to each other. Furthermore, the low-angle reflection is also kept. Figure 6 shows the WAXD powder patterns for all TPP(n=odd)s after the samples were cooled to room temperature at a cooling rate of 5 °C/min. Nevertheless, it is difficult to exactly identify the phase structure and type of order for these TPP(n=odd)s since a WAXD powder pattern does not provide locations of these reflections and therefore lacks the dimensionality of the ordered structure.

Phase Structure Identifications. Figures 7a−d, 8a−d, and 9a−d show three sets of WAXD fiber patterns for TPP(n=7, 11, and 15)s at temperatures slightly below those transition temperatures observed *via* DSC as well as at room temperature. Although these fiber patterns were taken during heating, we analyze them from high temperature to low temperature in order to follow the same sequence in the discussion of the previous results. For TPP(n=7) fibers below 178 °C, the WAXD fiber pattern (Figure 7a) shows that only one reflection peak existed on the equatorial at around $2\theta = 18.6(0)°$ (d-spacing of 0.48 nm) and has a correlation length of about 1.6 nm, representing a short range order. The low-angle reflection is not found. This clearly represents a nematic liquid crystal phase. After the temperature is below 137 °C, the WAXD pattern shows two reflections, both of which are in the quadrant. One of them is at $2\theta = 18.7(9)°$ (d-spacing of 0.472 nm) and is tilted 4° away from the equatorial. Another reflection is found in the quadrant with $2\theta = 19.4(0)°$ (d-spacing of 0.458 nm) and is tilted 14° away from the

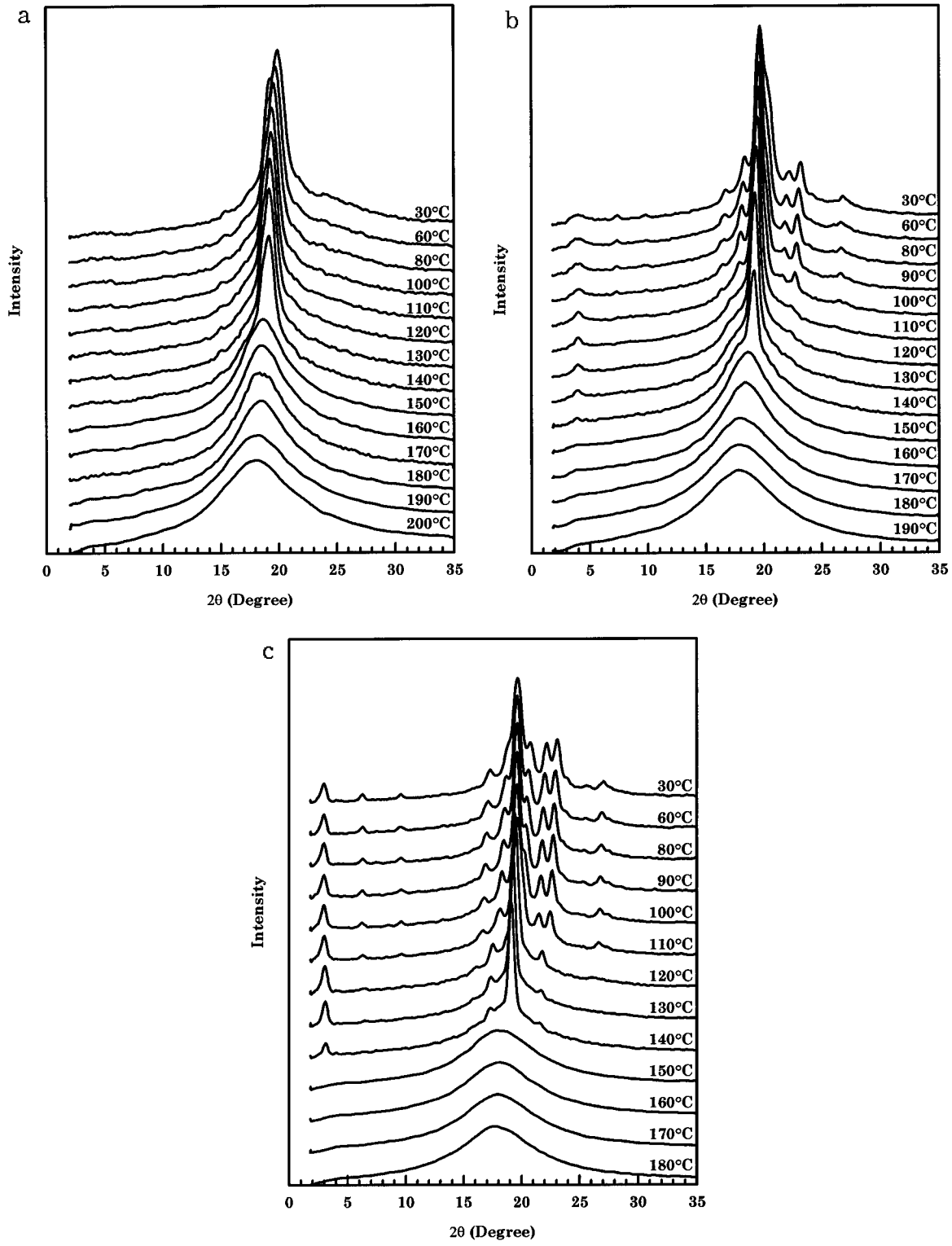

Figure 4. Sets of WAXD powder patterns during cooling from the isotropic melt at 5 °C/min for (a) TPP(n=7), (b) TPP(n=11), and (c) TPP(n=15).

equatorial. These are the two overlapped reflections observed in the WAXD powder pattern in Figure 4a. The correlation lengths of both reflections are 9.5 and 8.4 nm, respectively, and should be an indication of a quasi-long range order. However, this structure is close to being the long range order. The low-angle reflection of weak intensity at $2\theta = 5.4(0)°$ (d-spacing of 1.637 nm) appears. It is tilted at an angle of 44° away from the equatorial, indicating that the normal direction of the layer is tilted 46° from the meridian. Its correlation length is 4.9 nm, revealing that the layer structure exhibits a quasi-long range order. A reasonable explanation of this observation is that the first two reflections are attributed to two sets of the reflection planes, (110) and (200), when the chains possess a pseudohexagonal packing which can be recognized by viewing the direction parallel to the chain axis. Furthermore, the chain direction in the packing possesses a 32° angle with respect to the layer surfaces and the pseudohexagonal packing is tilted toward a side (the b-direction of the monoclinic packing, see below), and this brings 110 and 200 reflections out of the equatorial. The low-angle reflection is the (001) plane and is shown in Figure 10. It can therefore be assigned as a monoclinic unit cell

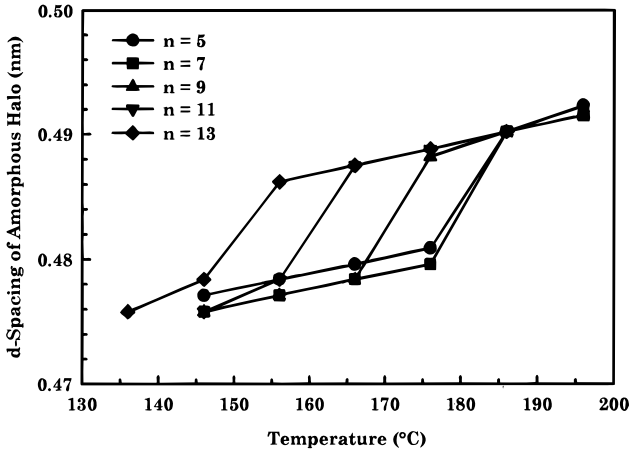

Figure 5. *d*-spacing shifts for TPP(*n*=odd)s during the highest temperature transitions observed in DSC (the nematic phase formation when $n \leq 13$).

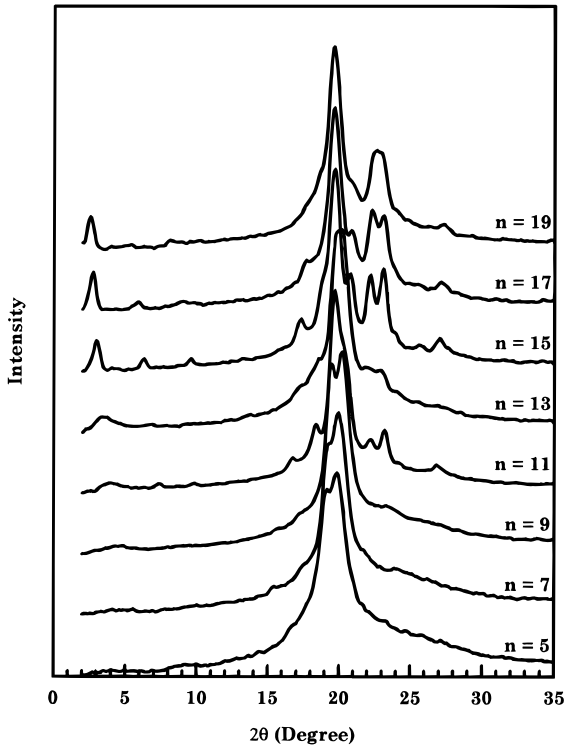

Figure 6. WAXD powder patterns of TPP(*n*=odd)s at 30 °C (a 5 °C/min cooling rate).

with $a = 1.08$ nm, $b = 0.551$ nm, $c = 1.93$ nm, and $\beta = 122°$. The chain direction is tilted 14° away from the fiber direction. The *c*-axis is slightly shorter than the length of one repeating unit with all the methylene units in the *trans* conformation. On the basis of this unit cell structure, a calculated WAXD fiber pattern can be obtained and this calculated pattern fits very well with the experimental one (Figure 7b). The detailed structure and molecular packing model for this calculation will be reported in the future publication. The normal directions of the (110) and (200) planes are clearly not perpendicular to the fiber direction but rather give rise to the reflections in the quadrant at 4 and 14° away from the equatorial. This phase can thus be assigned as a smectic F (S_F) phase based on the definition of small molecule liquid crystals.[16,17] In this case, a clear distinction can be made for this S_F phase from a smectic I (S_I) phase in which the chain molecules are tilted toward an apex. This is due to the fact that under such

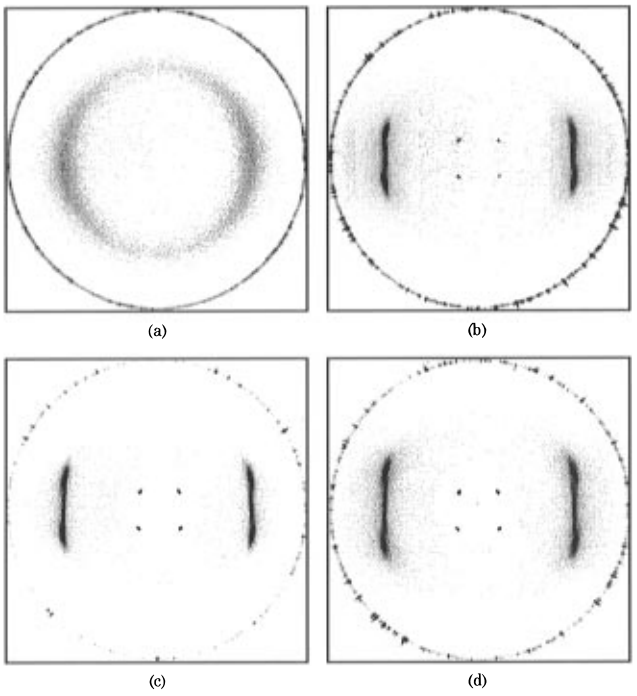

Figure 7. WAXD fiber patterns of TPP(*n*=7) at (a) 175 °C, (b) 135 °C, (c) 118 °C, and (d) 30 °C.

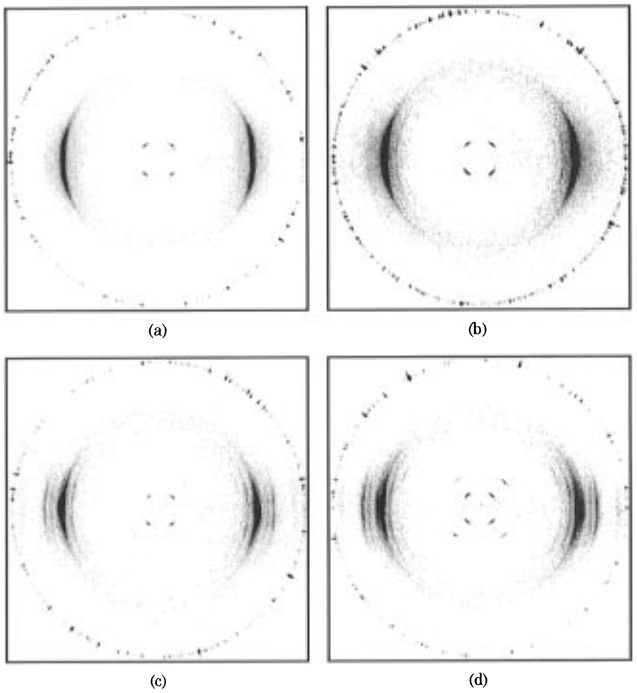

Figure 8. WAXD fiber patterns for TPP(*n*=11) at (a) 140 °C, (b) 135 °C, (c) 100 °C, and (d) 30 °C.

chain orientation the (020) reflection in the S_I phase must be located at the equatorial.[18]

Below the weak transition temperature of 129 °C, the TPP(*n*=7) WAXD fiber pattern (Figure 7c,d) only shows two major reflections in the wide angle region and one reflection in the small angle region. At 118 °C (Figure 7c) it is clear that the two wide angle reflections are $2\theta_{(110)} = 19.1(5)°$ (*d*-spacing of 0.463 nm) and $2\theta_{(200)} = 19.5(0)°$ (*d*-spacing of 0.455 nm). They are both tilted away from the equatorial, having angles of 8 and 16°, respectively, and possess respective correlation lengths of 12.8 and 10.2 nm (long range order, compared with those of 9.5 and 8.7 nm in the S_F case). The low-angle

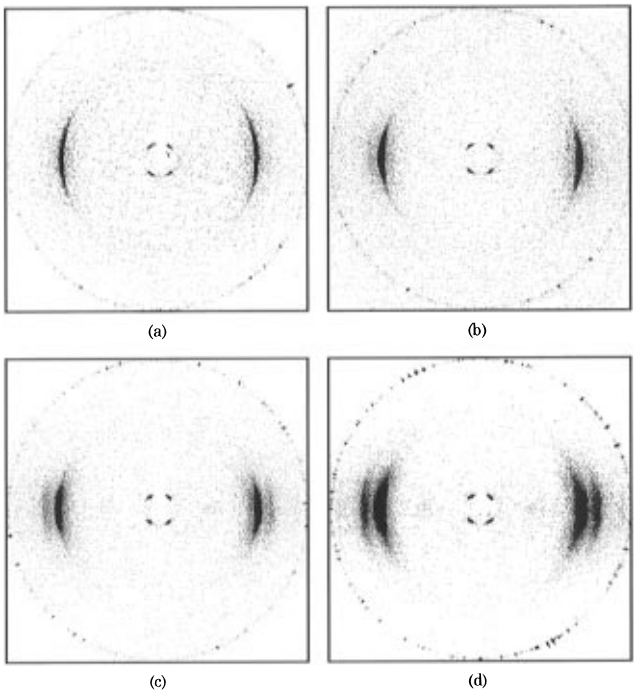

Figure 9. WAXD fiber patterns for TPP(n=15) at (a) 147 °C, (b) 130 °C, (c) 115 °C, and (d) 30 °C.

reflection at $2\theta_{(001)} = 5.4(0)°$ still remains and has a correlation length of 11.1 nm (long range order). Combining the powder WAXD patterns in Figures 4a and 7, reveals other minor reflections at $2\theta = 21.8(0)$ and 23.9(0)° in addition to these two major reflection peaks. This indicates that this S_F phase can be further ordered, most likely within the layers, to form smectic G (S_G) crytals. For TPP(n=7) a monoclinic unit cell with a = 1.05 nm, b = 0.538 nm, c = 1.89 nm, and $\beta = 120°$ can thus be identified and all the reflections fit into this lattice. The chain direction is tilted 16° away from the fiber direction. This can also be supported by the first-order transition with weak enthalpy and entropy changes at the transition, as shown in DSC experiments (Figures 1a). This agrees well with a general observation that the enthalpy change at the transition of $S_F \rightarrow S_G$ is weak (around 1 kJ/mol in small molecule liquid crystals[16]). Further experimental evidence to support the existence of the S_F and S_G phase transition can be found in the discontinuous change of the unit cell volume at the transition temperature for TPP($n \leq 9$)s.[18] This indicates that, indeed, at this temperature a thermodynamic first-order transition exists. Therefore, one may conclude that for TPP(n=7) the transition sequence during cooling is

$$\mathrm{I} \xrightarrow{178\ °\mathrm{C}} \mathrm{N} \xrightarrow{137\ °\mathrm{C}} \mathrm{S_F} \xrightarrow{129\ °\mathrm{C}} \mathrm{S_G}$$

Further decreasing the temperature leads to slight but continuous changes of the reflection peak positions due to thermal expansion.[18] This results in a slight, continuous shift of smectic packing parameters. However, the order of the S_G phase is essentially not changed. This transition sequence is also held for TPP($n \leq 9$)s.

On the other hand, for TPP(n=11), the WAXD fiber pattern at the temperature below the highest transition temperature of 165 °C shows one broad reflection on the equatorial at $2\theta = 18.5(4)°$. The correlation length of this reflection is 1.7 nm, revealing a short range order. On the basis of the shift of the d-spacing of this reflection at the transition temperature (Figure 5), it is

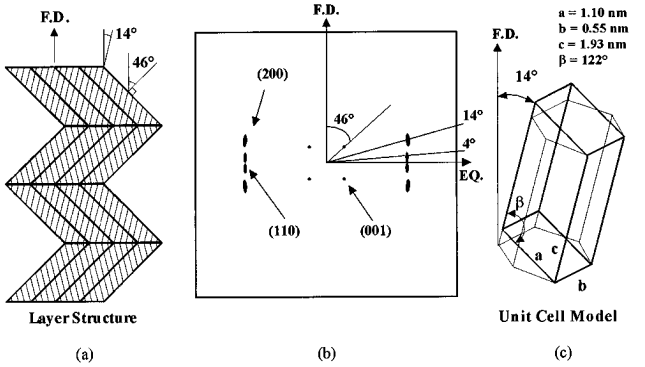

Figure 10. Chain packing model of TPP(n=7) in the S_F phase: (a) layer structure; (b) WAXD fiber pattern; and (c) unit cell. (FD is the fiber direction, and EQ is the equator.)

evident that the 165 °C transition represents the I → N phase transition. Temperatures below 146 °C lead to WAXD fiber patterns as shown in Figure 8a). This pattern is very similar to that of S_F in TPP($n \leq 9$)s in that it has two major reflections on the quadrant at $2\theta_{(110)} = 19.1(0)°$ (d-spacing of 0.465 nm) and $2\theta_{(200)} = 19.3(0)°$ (d-spacing of 0.460 nm), which are tilted 3 and 7° away from the equatorial, respectively. The correlation lengths are 11.3 and 10.6 nm, revealing the existence of long range order but are close to the quasi-long range order side. The low-angle reflection at $2\theta_{(001)} = 4.20(0)°$ (d-spacing of 2.10 nm) appears in the quadrant at an angle of 48° away from the equatorial, and its correlation length is 5.9 nm (quasi-long range order). A monoclinic unit cell having a = 1.123 nm, b = 0.539 nm, c = 2.57 nm, and $\beta = 125°$ can be determined. This is, again, a S_F phase with the chains tilting toward one side. The chain direction is 7° away from the fiber direction.

At temperatures below 135 °C, one more reflection appears in the quadrant (Figure 8b). Detailed analysis indicates that there are two reflections on the equatorial at $2\theta_{(110)} = 19.2(0)°$ and $2\theta_{(200)} = 19.4(0)°$ (d-spacings of 0.462 and 0.458 nm, respectively), having correlation lengths of 13.8 and 11.9 nm (long range order). The reflection in the quadrant is at $2\theta_{(\bar{2}01)} = 17.2(5)°$ (d-spacing of 0.510 nm), having a correlation length of 12.3 nm. This indicates that three-dimensional order exists within the layers. The low-angle reflection of (001) planes exhibiting a strong intensity with a d-spacing of 2.10 nm is located in the quadrant and is tilted at an angle of 55° from the equatorial. Therefore, the normal direction of the layer is tilted 35° from the meridian direction. The correlation length of this reflection is 27.3 nm. X-ray analysis shows that all these reflections can be fit into a monoclinic unit cell with a = 1.13 nm, b = 0.536 nm, c = 2.60 nm, and $\beta = 126°$. The chain direction is tilted 5° from the fiber direction. As a result, it should be a S_G phase based on the nomenclature for small molecular liquid crystals.[16,17]

When the temperature is below 105 °C for TPP(n=11), as shown in Figure 8c,d, the layer structure having the correlation length of 12.6 nm still exists, as evidenced by the sharp reflection at $2\theta_{(001)} = 4.1(0)°$ (d-spacing of 2.16 nm) with a tilt angle of 50° from the fiber direction. The second-order reflection of the layer spacing at $2\theta_{(002)} = 8.1(0)°$ can also be seen. Three reflections are found on the equatorial at $2\theta = 19.6(0)$, 20.10(0), and 26.3(1)° for (200), (110), and (210) planes, respectively, in which the second one possesses the major intensity. Four reflections appear in the quadrant besides the (001) reflection. Three of them are on the first layer and one

is on the second layer. They are at $2\theta = 17.7(1)$, 21.3(3), 23.0(0), and 16.5(7)° for (201), (111), (201), and (102) planes, respectively. The correlation lengths of all these reflections indicate long range order (>10 nm). On the basis of the reciprocal lattice, a monoclinic unit cell of $a = 1.153$ nm, $b = 0.528$ nn, $c = 2.81$ nm, and $\beta = 130°$ can be obtained. The chain direction is now parallel to the fiber direction. In this phase a herringbone orthorhombic packing is found when the viewing direction is parallel to the chain direction and the lattice is tilted toward the short *b*-axis side. This structure can be assigned as a smectic H (S_H) crystal.[16,17] The 103 °C transition is thus the $S_G \rightarrow S_H$ transition. For TPP(n=11) the phase transition sequence during cooling can thus be

$$I \xrightarrow{165\ °C} N \xrightarrow{146\ °C} S_F \xrightarrow{135\ °C} S_G \xrightarrow{105\ °C} S_H$$

It is also found that TPP(n=13) possesses the same transition sequence.

For TPP(n=15), a similar structural analysis can be carried out. Below the highest transition temperature of 150 °C (Figure 9a), one reflection can be observed on the equatorial at $2\theta_{(100),(200)} = 19.4(0)°$ (d-spacing of 0.458 nm). A low-angle reflection at $2\theta_{(001)} = 3.5(0)°$ (d-spacing of 2.52 nm) is located at the first layer and it is sharp and clear. Two additional reflections are in the same layer of the quadrant. This WAXD fiber pattern indicates a S_F phase having a monoclinic unit cell with $a = 1.13$ nm, $b = 0.528$ nm, $c = 3.12$ nm, and $\beta = 126$ °C. Note that, in this case, the chain orientation is parallel to the fiber direction and therefore the (200) and (110) planes are superimposed with each other. The correlation length of these planes is 14.9 nm. The low-angle reflection possesses a correlation length of 14.7 nm, revealing long range order. At the temperature of 129 °C, another transition has been passed, as shown in the DSC results. Figure 9b is the WAXD fiber pattern. All the reflections in the S_F remain, and additional minor reflections can be found. A S_G phase is assigned for this further ordering process, and it defines a monoclinic unit cell having $a = 1.16$ nm, $b = 0.526$ nm, $c = 3.20$ nm, and $\beta = 128°$. The correlation lengths are all in the long range order region (>10 nm). After the temperature is lower than 118 °C, the WAXD fiber patterns show 12 reflections in Figure 9c,d. Careful calculation based on the reciprocal lattice leads to identification of a S_H crystal phase having a monoclinic unit cell with $a = 1.11$ nm, $b = 0.526$ nm, $c = 3.25$ nm, and $\beta = 128°$.[18] When the viewing direction is parallel to the chain direction, a herringbone orthorhombic packing is again found. The phase transition sequence during cooling is thus

$$I \xrightarrow{150\ °C} S_F \xrightarrow{129\ °C} S_G \xrightarrow{118\ °C} S_H$$

This transition sequence is also held for TPP($n \geq 15$)s.

Morphological Evidence of the Phase Transitions. Parts a−c of Figure 11 show morphological observations of TPP(n=7) without mechanical shearing and TPP(n=7 and 15) with mechanical shearing. In the normal observations, the sample becomes immediately birefringent after a few seconds at temperatures 1 or 2 deg below the highest transition temperature. A fine, grainy texture type of pattern is typical for all TPP(n=odd)s (Figures 11a). However, after the mechanical shearing and slight relaxation banded textures can be found in TPP($n \leq 13$)s. This banded texture which has

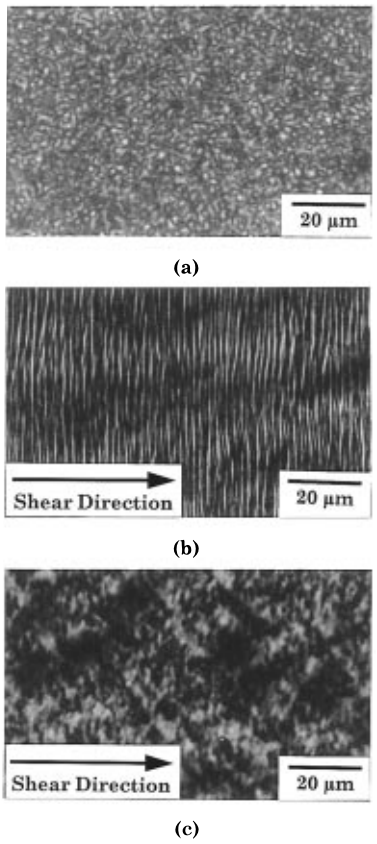

Figure 11. PLM morphological observations of (a) TPP(n=7) without mechanical shearing and (b and c) TPP(n=7 and 15) with mechanical shearing.

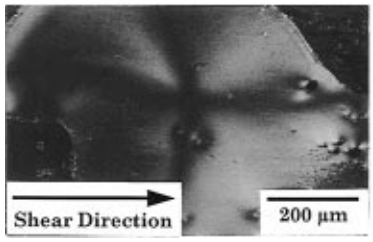

Figure 12. PLM observation of liquid crystalline defects in monodomains of TPP(n=7) under a strong mechanical shear force field.

a spacing of about 1 μm is perpendicular to the shear direction (Figure 11b). The fact that banded texture appears under an external force field has been viewed as a typical orientationally ordered liquid crystalline polymer pattern in the N, S_A, or S_C phase.[6,19−21] Microscopic analysis has shown that, in the banded texture, the director continuously oscillates spatially about the direction imposed by the previous flow. On the other hand, Figure 11c shows no clear banded texture under PLM. Instead, a schlieren-mosaic type of texture is seen, indicating that the highly ordered S_F phase possesses a structure closer to the solid state and the regular banded texture is more difficult to form. Under a strong mechanical, periodic shear force field, micrometer-size monodomains may also form in these TPP ($n \leq 13$)s in the nematic liquid crystalline temperature range. Observable size defects in the schlieren texture can be found as shown in Figure 12. This defect is a point singularity with four brushes, $s = +1$ defect, based on the definition proposed by Oseen[22] and Frank.[23] Further decreasing the temperature does not show a significant PLM morphological change, but a birefringence change is observed. The precursor texture still

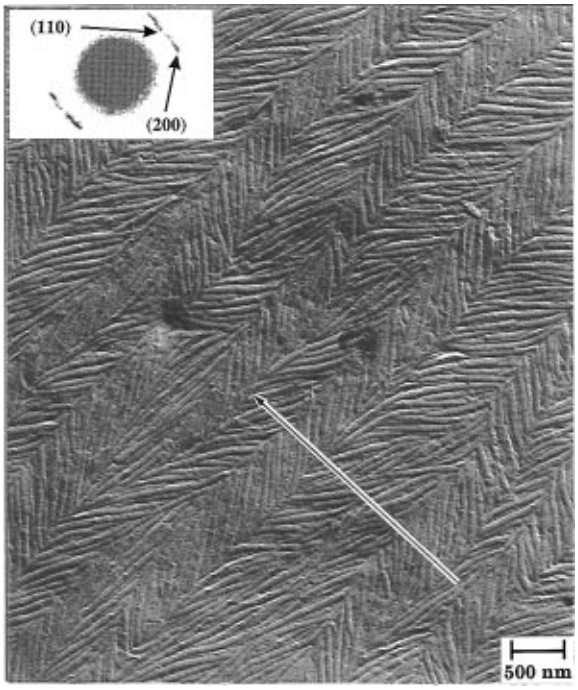

Figure 13. TEM observation of mechanically sheared TPP(n=7) after lamellar decoration. An electron diffraction pattern is also included.

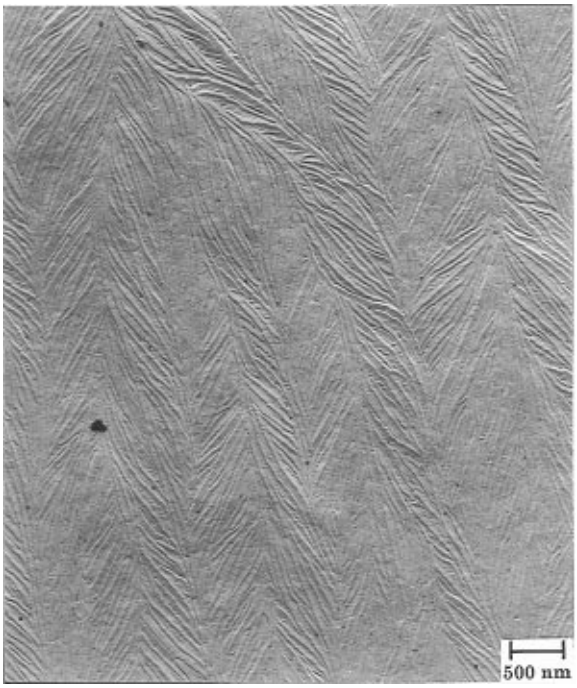

Figure 14. TEM observation of mechanically sheared TPP(n=11) after lamellar decoration.

remains even at room temperature. This indicates that the ordered structure change occurs at even smaller dimensional scale (within micrometer size).

Using the "lamellar decoration method" originally developed by Thomas *et al.*,[12,13] the morphology of the liquid crystals possessing highly ordered structure may be observed under TEM. However, it should be pointed out that the observed morphology is critically dependent upon the precursor phase. Therefore, if one wants to find the morphology of a S_F phase without inteference of the morphologies from other liquid crystalline phases, this phase has to be developed directly from the isotropic melt. As a result, only TPP($n \geq 15$)s provide this kind of observation. In Figure 13, TPP(n=7) was mechanically sheared in the nematic phase (the shear direction is indicated in the figure) and annealed at a temperature slightly lower than the lowest transition temperature. It is clear that the lamellar normal direction is $\pm 46(\pm 2)°$ with respect to the shear direction. This is responsible for the four point reflections in the low-angle region observed from the WAXD fiber pattern (Figure 7b−d). The lamellar spacing is around 50 nm, and this size is greater than the correlation length obtained from the WAXD experiments, which are in the vicinity of 10−15 nm for TPP(n=7 and 11) in the S_G and S_H phases at room temperature. The layer spacing of about 0.5−1 μm in the TEM observations clearly corresponds to the banded texture found in PLM (Figure 11b). The shear direction is interestingly perpendicular to the layer texture, as indicated by the ED pattern, revealing a zigzag-like morphological arrangement. Furthermore, the d-spacing and location of the reflection spots in the ED pattern is essentially the same as those found in the WAXD fiber pattern in Figure 7d. This indicates that the local orientation and order are the same as the overall ones detected *via* WAXD experiments. A similar texture can be found for sheared TPP(n=11), as shown in Figure 14.

Generally speaking, a layer compression in a highly ordered smectic liquid crystalline phase requires considerable energy, while the deformations that tend to preserve the interlayer spacing may still be possible. The expected distortion is thus the layer bending since this involves only a splaying effect and does not affect the layer thickness.[24] As a result, for defects formed in this phase the splay elastic constant (k_{11}) should dominate, while the twist deformation (k_{22}) and the bend elastic constant (k_{33}) must be very small. This leads to a remarkable anisotropic response to different types of deformation in the samples. In Figures 13 and 14 the mechanically sheared TPP thin sample prepared from these smectic phases is more or less planar. This indicates that the chain molecules are homogeneous. Since the layer structures are tilted, the molecules have two different layer orientations with respect to the shear direction. It is particularly interesting that the lamellar orientations are more or less alternated along the shear direction to form a zigzag-like texture. This may be the cause of the π inversion or other tilted wells. In some cases, nonplanar texture can also be found such as focal conic and chevron textures.[16,25] Detailed defect analysis and morphological discussion will be reported elsewhere.[26]

Finally, the S_F morphology and defects after the mechanical shearing are shown in Figure 15 for TPP(n=15). This phase is directly formed from the isotropic melt after the sample was cooled for 170 to 140 °C (see Figure 2) and, therefore, no morphology and defects of the precursor phase interfere with this observation. There is clear evidence of a lamellar texture with a spacing of about 50 nm, and the lamellar orientation is tilted with the shear direction. However, no obvious regular zigzag-like banded texture can be found. This corresponds well with the PLM observation where no banded texture is observed (Figure 11c).

Phase Diagram of TPP(n-odd)s. On the basis of these experimental observations in TPP(n=odd)s, we can clearly assign the phase structure in the phase diagram (Figure 2) by following the sequence from high to low temperatures. The first (and the highest) transition is the I → N phase transition for TPP($n \leq 13$)s, while

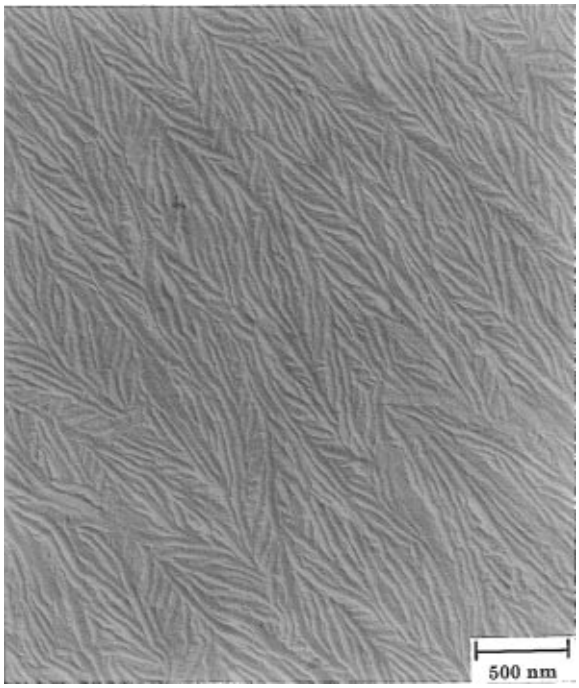

Figure 15. TEM observation of mechanically sheared TPP-(n=15) after lamellar decoration.

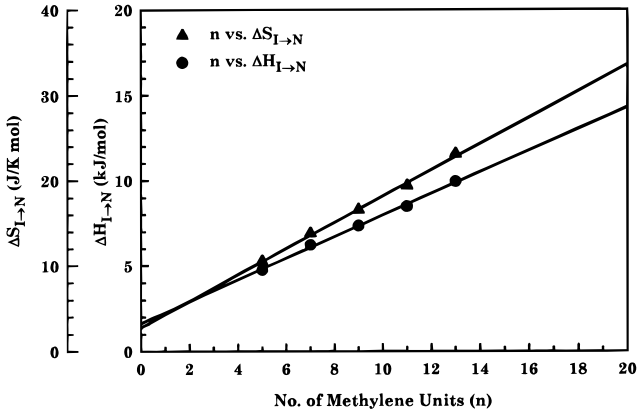

Figure 16. Relationships between the enthalpy and the entropy changes during the I → N transitions observed in DSC and the number of methylene units for TPP($n\leq13$)s.

a transition from the I → S_F phase can be observed during the highest temperature transition for TPP-($n\geq15$)s. With decreasing temperature, a S_F phase is found in TPP($n\leq13$)s in a rather narrow temperature range. This S_F phase for all TPP(n=odd)s transforms to the S_G phase and, finally, for TPP($n\geq11$), a S_H phase ultimately forms as the most thermodynamically stable phase before reaching the glass transition temperatures.

Furthermore, one may also investigate the enthalpy changes of transitions for the TPP(n=odd)s to support this assignment. The enthalpy changes of the I → N transition for TPP($n\leq13$)s are plotted with the number of methylene units as shown in Figure 16. Since their transition temperatures are close to equilibrium, the transition entropy change can thus be calculated and plotted in the same figure. It is interesting that with the increasing number of methylene units, this enthalpy change at the transition linearly increases [having a slope of 0.63 kJ/(mol of methylene units)] in this range of the number of the methylene units. This clearly reveals that the methylene units also join the ordering process during this transition and the slope roughly represents the contribution to the nematic order for each

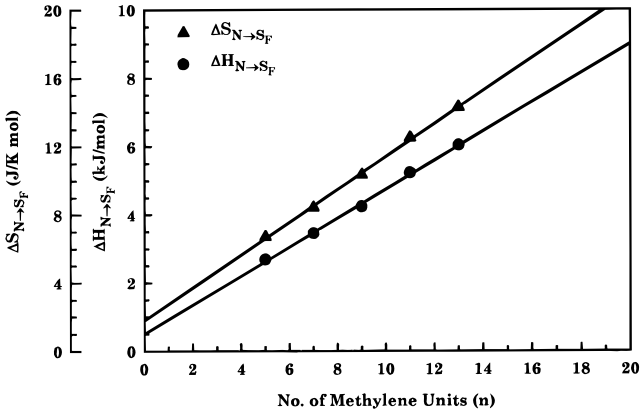

Figure 17. Relationships between the enthalpy and the entropy changes during the N → S_F transitions observed in DSC and the number of methylene units for TPP($n\leq13$)s.

methylene unit. The entropy change of each methylene unit at the transition is 1.54 J/(K mol). An extrapolation to zero methylene unit yields the enthalpy change of this transition for the pure mesogenic group at the transition which is 1.64 kJ/mol. The entropy change of the mesogenic group alone at the transition obtained from the extrapolation is 2.80 J/(K mol). Generally speaking, the enthalpy and entropy changes of a liquid crystalline transition dependent upon the structural rigidity, symmetry, planarity, and length of the mesogenic groups, all of which are essential to stabilize the liquid crystalline phase. If the mesogenic groups are not able to provide enough stability to the liquid crystalline phase, the methylene units may have to provide more contributions to it. Sometimes the liquid crystalline transition may even change from the enantiotropic to a monotropic type before the liquid crystalline phase is completely destabilized. This case has been found in polyethers (MBPE) synthesized from 1-(4-hydroxyphenyl)-2-(2-methyl-4-hydroxyphenyl)ethane and α,ω-dibromoalkanes[14] and poly(ester imide)s (PEIM) synthesized from *N*-[4-(chloroformyl)phenyl]-4-(chloroformyl)phthalimide and different diols,[6] both of which only exhibit monotropic liquid crystalline behaviors. However, the absolute values of the enthalpy and entropy changes of this nematic liquid crystalline transition in TPP(n=odd)s are even higher than those commonly found in enantiotropic liquid crystalline polymers such as in the case of (4,4′-dihydroxy-2,2′-dimethylazoxybenzene)alkanedioic acid (ME9-Sn). The enthalpy changes of transition for the odd-numbered ME9-Sns are 0.19 kJ/mol for each methylene unit and 0.94 kJ/mol for the mesogenic group, while their entropy changes during the transition are 0.57 and 1.41 J/(K mol), respectively.[27,28] This may indicate that in TPP(n=odd)s the thermodynamic stability of this liquid crystalline phase is high. On the other hand, the enthalpy and entropy changes of the N → S_F transition for TPP($n\leq13$)s (Figure 17) indicate that the methylene units still take part in the ordering process involving a contribution of the enthalpy change of transition of 0.43 kJ/mol and an entropy change of 0.96 J/(K mol) for each methylene unit. The extrapolated values for the enthalpy and entropy changes during this transition for pure mesogenic groups are 0.50 kJ/mol and 1.78 J/(K mol), respectively.

For TPP($n\geq15$)s, the S_F phase appears after passing through the highest transition temperature (Figure 2) and therefore the enthalpy and entropy changes of transition cannot be included in Figure 16. The rela-

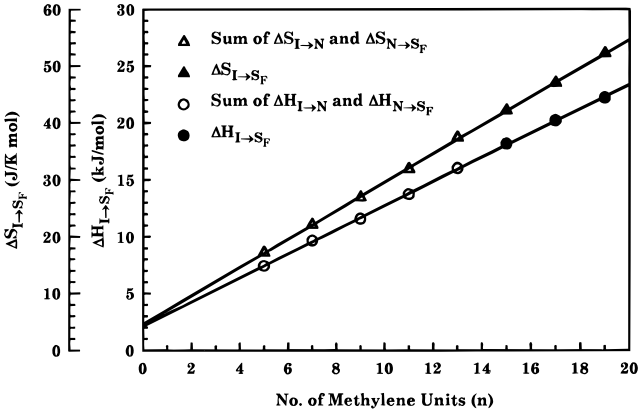

Figure 18. Relationships between the enthalpy and the entropy changes during the I → S_F transitions observed in DSC and the number of methylene units for TPP($n \leq 15$)s. Those of summations of I → N and N → S_F transitions for TPP($n \leq 13$)s are also included.

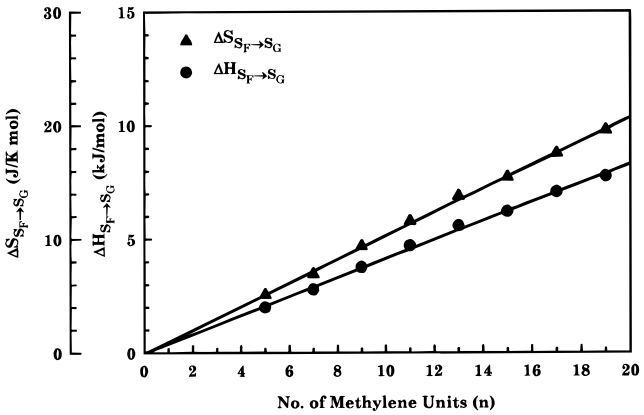

Figure 19. Relationships between the enthalpy and the entropy changes during the S_F → S_G transitions observed in DSC and the number of methylene units for TPP(n=odd)s.

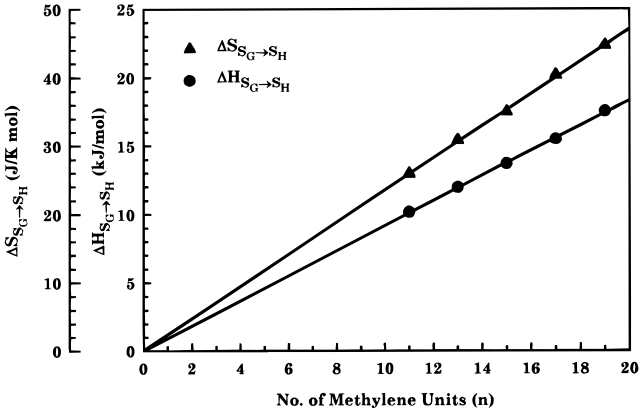

Figure 20. Relationships between the enthalpy and the entropy changes during the S_G → S_H transitions observed in DSC and the number of methylene units for TPP($n \geq 11$)s.

tionship between the enthalpy changes of the I → S_F transition and the number of the methylene units is shown in Figure 18. Furthermore, one expects that the summation of the thermodynamic parameters in TPP($n \leq 13$)s where two consecutive transitions are taking place (I → N and N → S_F) should fit the same relationships as those of the single-step I → S_F transitions for TPP($n \geq 15$)s. The data are shown in Figure 18, and indeed, both sets of enthalpy and entropy changes for all TPP(n=odd)s fit very well in the same linear line. This indicates that the additivity assumption proposed is held. The enthalpy and entropy changes per methylene unit obtained from Figure 18 are 1.06 kJ/mol and 2.50 J/(K mol), respectively. Those of the mesogenic group are 2.14 kJ/mol and 4.58 J/(K mol). This indicates that the S_F structure having the tilted chain direction with respect to the fiber direction in TPP($n \leq 13$) possesses the same structural order compared to those of TPP($n \geq 15$) based on the thermodynamic considerations.

When one discusses the transitions of S_F → S_G for all TPP(n=odd)s, Figure 19 shows the relationships of the enthalpy and entropy changes with the number of methylene units; both changes per methylene unit are 0.42 kJ/mol and 1.04 J/(K mol), respectively, and the changes for the mesogenic groups are close to zero. This implies that, during this transition, the ordering process is solely occurring in the methylene units. Furthermore, it also indicates that in the S_G phase the tilted chain direction with the fiber direction does not affect the structural order.

Finally, the enthalpy and entropy changes during the S_G → S_H transition for TPP($n \geq 11$)s at different methylene units are plotted in Figure 20. It is evident that the intersections of both extrapolations to zero methylene units are also very close to zero, while the slopes of these two linear relationships are 0.92 kJ/mol for the enthalpy change and 2.36 J/(K mol) for the entropy change per methylene unit, respectively. This is an indication that the transition of S_G → S_H is also solely dependent upon the further ordering of the methylene units. All the enthalpy and entropy changes at those transitions are listed in Table 1 for the purpose of comparison and discussion.

Table 1. Mesogenic Group and Methylene Unit Contributions to the Liquid Crystalline Transitions

	ΔH (kJ/mol)		ΔS [J/(K mol)]	
transitions	meso-gene	methyl-ene	meso-gene	methyl-ene
I → N for TPP($n \leq 13$)s	1.64	0.63	2.80	1.54
N → S_F for TPP($n \leq 13$)s	0.50	0.43	1.78	0.96
I → S_F for TPP($n \geq 15$)s	2.14	1.06	4.58	2.50
S_F → S_G	≈0.00	0.42	≈0.00	1.04
S_G → S_H for TPP($n \geq 11$)s	≈0.00	0.92	≈0.00	2.35

Conclusion

We have reported a phase diagram of TPP(n=odd) liquid crystalline polyethers. These polymers possess complicated phase behavior. The thermodynamic properties are observed *via* DSC experiments, which provide fundamental judgments of the phase stability and sometimes an additional proof of the phase assignments. However, the essential structural information has to be obtained through WAXD powder and fiber patterns at different temperatures, combined with PLM and TEM morphological observations. The interesting results are the identification of highly ordered smectic crystals (the S_F, S_G, and S_H phases) which also exist in main chain liquid crystalline polymers. It is thus necessary to carefully examine the polymer liquid crystalline structures and identify these highly ordered smectic liquid crystalline phases based on structural symmetry, order, morphology, and defects, which should be similar to those in small molecule liquid crystals. In this TPP(n=odd) case, it is further understood that in the S_F and S_G phases an orientational difference between the chain and fiber directions in the WAXD fiber patterns can be found but the structural order is not affected. Finally, it should also be pointed out that growing liquid

crystalline monodomains in these polymers is the ideal situation to identify the highly ordered smectic phases. Unfortunately, it is very difficult to obtain them experimentally due to the long chain nature.

Acknowledgment. This research was supported by S.Z.D.C.'s Presidential Young Investigator Award (DMR-9157738).

References and Notes

(1) For a recent review, see for example: Percec, V.; Tomazos, D. In *Comprehensive Polymer Science*; Allen, G., Aggarwal, S. L., Russo, S., Eds.; Pergamon: Oxford, U.K. 1992; First Supplement, pp. 300−356. In this review, over four hundred references were collected.
(2) Meurisse, P.; Noel, C.; Monnerie, L.; Fayolle, B. *Br. Polym. J.* **1981**, *13*, 55.
(3) Ober, C.; Jin, J.-I.; Lenz, R. W. *Polym. J. (Jpn.)* **1982**, *14*, 9.
(4) Krigbaum, W. R.; Asrar, J.; Toriumi, H.; Ciferri, A.; Preston, J. *J. Polym. Sci., Polym. Lett.* **1982**, *20*, 109.
(5) Pardey, R.; Harris, F. W.; Cheng, S. Z. D.; Aducci, J.; Facinelli, J. V.; Lenz, R. W. *Macromolecules* **1992**, *25*, 5060.
(6) Pardey, R.; Harris, F. W.; Cheng, S. Z. D.; Aducci, J.; Facinelli, J. V.; Lenz, R. W. *Macromolecules* **1993**, *26*, 3687.
(7) Pardey, R.; Harris, F. W.; Cheng, S. Z. D.; Keller, A.; Aducci, J.; Facinelli, J. V.; Lenz, R. W. *Macromolecules* **1994**, *27*, 5794.
(8) Yoon, D. Y.; Masciocchi, N.; Depero, L. E.; Viney, C.; Parrish, W. *Macromolecules* **1990**, *23*, 1793.
(9) Coassolo, A.; Foá, M.; Dainelli, D.; Scordamaglia, R.; Barino, L.; Chapoy, L. L.; Rustichelli, F.; Yang, B.; Torquati, G. *Macromolecules* **1991**, *24*, 1701.
(10) Carotenuto, M.; Iannelli, P. *Macromolecules* **1992**, *25*, 4373.
(11) Percec, V.; Chu, P.; Ungar, G.; Cheng, S. Z. D.; Yoon, C.-Y. *J. Mater. Chem.* **1994**, *4*, 719.
(12) Thomas, E. L.; Wood, B. A. *Faraday Discuss. Chem. Soc.* **1985**, *79*, 229.
(13) Wood, B. A.; Thomas, E. L. *Nature* **1986**, *324*, 655.
(14) Yandrasits, M. A.; Cheng, S. Z. D.; Zhang, A.-Q.; Cheng, J.-L.; Wunderlich, B.; Percec, V. *Macromolecules* **1992**, *25*, 2112.
(15) Ungar, G.; Feijoo, J. L.; Keller, A.; Yourd, R.; Percec, V. Macromolecules **1990**, *23*, 244.
(16) Gray, G. W.; Goodby, J. W. G. *Smectic Liquid Crystals*; Leonard Hill: London, 1984.
(17) Pershan, P. S. *Structure of Liquid Crystal Phases*; World Scientific: Teaneck, NJ, 1988.
(18) Cheng, S. Z. D.; Yoon, Y.; Zhang, A.-Q.; Savitski, E. P.; Park, J.-Y.; Percec, V.; Chu, P. *Macromol. Rapid Commun.* **1995**, *16*, 533.
(19) Kiss, G.; Porter, R. S. *Mol. Cryst. Liq. Cryst.* **1980**, *60*, 267.
(20) Donald, A. M.; Viney, C.; Windle, A. H. *Polymer* **1983**, *24*, 155.
(21) Chen, J.-H.; Zhang, A.-Q.; Yandrasites, M. A.; Cheng, S. Z. D.; Percec, V. *Makromol. Chem.* **1993**, *194*, 3135.
(22) Oseen, C. W. *Fortsschr. Chem. Phys., Phys. Chem.* **1929**, *29*, 1. See also: *Trans. Faraday Soc.* **1933**, *29*, 883.
(23) Frank, F. C. *Discuss. Faraday Soc.* **1958**, *25*, 19.
(24) Chandrasekhar, S. *Liquid Crystals*, 2nd ed.; Cambridge University Press: Cambridge, U.K., 1992; Chapter 5.
(25) Demus, D.; Richter, L. *Textures of Liquid Crystals*; Verlag Chemie: New York, 1978.
(26) Yoon, Y. Ph.D. Dissertation, Department of Polymer Science, The University of Akron, Akron, Ohio 44325-3909, 1995.
(27) Blumstein, A.; Thomas. O. *Macromolecules* **1982**, *15*, 1264.
(28) Blumstein, R. B.; Blumstein, A. *Mol. Cryst. Liq. Cryst.* **1988**, *165*, 361.

MA950238L